Correlative light and electron microscopy : strategies and applications

Driel, L.F. van

Chapter 6

Discussion and Outlook:

Exploring the Boundaries of Correlative Microscopy

6.1. Introduction

One aim of structural cell biology is to determine the three dimensional (3D) organization of cells and tissues, under healthy and pathological conditions, down to the spatial resolution level needed to understand the structure and dynamics of macromolecular machines. At the same time, it is important to associate the structures with a defined physiological state and function. Although this goal is far from reached, many technical advances in the field of electron microscopy (EM) make this goal more and more realistic. For instance, an enormous progress is made in EM techniques like immuno-gold labeling for the localization of specific antigens (Koster and Klumperman, 2003; Peters and Pierson, 2008; Slot and Geuze, 2007), electron tomography for the 3D imaging of cells and tissues (Barcena and Koster, 2009; Frey et al., 2006; McIntosh et al., 2005), single particle analysis for high resolution 3D imaging of macromolecular complexes (Baumeister and Steven, 2000; Chiu et al., 2005; Grigorieff and Harrison, 2011), and the range of possibilities to image frozen hydrated specimens (Koning and Koster, 2009; Lucic et al., 2005; Zuber et al., 2008).

Technical developments that reach beyond the limits of EM, are the rapidly evolving diversity of correlative light and electron microscopy (CLEM) approaches. CLEM is powerful in identifying specific structures or molecules within structurally complex biological materials and therefore complements electron microscopy (EM) in one of its weakest qualities.

Although EM provides contrast and detail at high magnifications, at lower magnifications not more than a blur is observed. The same holds for relatively thin (< 100 nm) samples versus thick (> 500 nm) samples; thicker samples reveal much less morphological detail. The lack of details is due to the fact that the high resolution 3D features overlap in a 2D projection. The effects of magnification and sample thickness are especially prominent in EM specimens that lack stains, such as vitreous samples. It makes navigation through the cell, and identification of structures of interest, especially when they are rare, a time-consuming and often tedious activity. In practical circumstances, it often occurs that a large number of (cryo-) electron tomograms are taken with the hope that one of these tomograms will contain the structure of interest.

Fluorescence light microscopy (FM), on the other hand, excels in the navigation in cells and tissues, and the identification of rare events. Fluorescent labels can pinpoint at low magnification exactly where specific structures or macromolecular complexes are located. An additional opportunity of light microscopy in general is that it can offer a temporal dimension to a molecule of interest by performing live cell imaging. Ultimately, classical dilemmas in EM - like are we observing fusion or fission of membranes? - could hereby be avoided.

CLEM techniques described in this thesis

In this thesis, we explored several technical implementations of CLEM. Chapter 2 discussed the staining of ultrathin EM sections with LM dyes. The dyes facilitated orientation in complex tissue samples, like intestinal tissue and tissue from an aneurysm, and it offered a way to identify rarely occurring cells of interest. In chapter 3, LM is performed on fixed cell monolayers, and followed by transmission EM (TEM) of the sectioned material, or scanning EM (SEM) of the surface of the cells. The technique enabled the localization of exocytosed vWF, and the subsequent identification of the ultrastructural origin of these secreted protein.

Chapter 4 described a workflow that enables cryo-CLEM. The workflow includes a dedicated specimen stage to perform LM on vitreous samples, and a software tool to retrace the observed LM features in cryo-EM. Of all the CLEM techniques that have been described, its application to unstained vitrified structures (cryo-CLEM) speaks most to the imagination concerning the value it can add to TEM alone. Cryo-EM is a technique that demands considerable EM resources and operator skills, due to the inherent low signal-to-noise ratio and the electron radiation sensitivity of frozen hydrated samples. And even when resources and operators are present, the search for a structure of interest in cryo-EM is best compared to the proverbial search for a needle in a haystack. In chapter five, the added value of the cryo-CLEM technique is illustrated by imaging pancreatic homogenates that were fluorescently labeled for filamentous actin. The workflow described in chapter 4 enabled the identification of actin coated zymogen granules, which were both rarely present in the sample and hardly identifiable by 2D cryo-EM.

6.2. Cryo-CLEM methodologies

Conceptionally, cryo-CLEM is rather straightforward: a specific structure of interest is identified by FM, and then traced in cryo-EM for its ultrastructural examination at the required level of detail. In reality, however, the workflow comes with several challenges. Most notably, it generally requires that for light microscopy the specimen is also imaged at cryogenic temperatures. The following two methodologies allow cryo-fluorescence imaging in combination with cryo-CLEM.

6.2.1. Cryo-fluorescence stage

Although low-temperature light microscopy (LM) stages have been commercially available for some time, they are not equipped to carry TEM specimen carriers (EM grids), and neither to handle vitreous samples. Therefore, during the last five years our group, as well as several other groups, developed stages for cryo-FM of EM samples. The stages were developed either “from scratch” with novel designs (Sartori et al., 2007; Schwartz et al., 2007), or modified from a commercially available low-temperature stage (chapter 4). Today, these stages are compatible with most conventional FM setups, either inverted (Rigort et al., 2010) or upright microscopes (Schwartz et al., 2007; chapter 4).

For the cryo-FM stage developed in our lab, we chose to modify the commercially available Linkam THMS 600 stage. As we described in chapter 4, the sample and the silver block support are cooled by LN_2 pumped from a Dewar into the silver block. The evaporated N_2 is recycled and used to purge the specimen chamber. The temperature of the silver block is monitored with a platinum resistor sensor and regulated by a controller. Prior to its modification, the Linkam THMS 600 stage held a specimen on a circular glass coverslip that is clamped in a stainless steel specimen-loading cartridge. The cartridge can be brought into the stage via a side-entry port. During our technical modifications, the coverslip was replaced by a 0.8 mm thick brass disc with a circular depression of 3 mm diameter in the center. The EM grid was held tightly in the circular depression by a pivoting clamp mechanism (that we removed from a room temperature EM specimen holder). To load an EM grid under LN_2, we designed a dedicated Styrofoam box that supports compartments for the loading cartridge and grid storage boxes. The box could be placed over the side-entry port of the cryo-FM stage with the purpose to minimize the amount of ice contamination on the EM grid when it is transferred in the cartridge from the LN_2 into the stage. The top of the stage was closed with a lid containing a Teflon objective collar, through which an objective lens entered to image the sample. Using a Leica 100x, NA 0.75 dry objective lens with a working distance of 4.7 mm, a resolution of 400 nm was obtained.

Since its publication in 2009, the cryo-FM stage has been improved in collaboration with the company Linkam (Surrey, UK) to improve its performance and allow fluorescence as well as

transmitted light imaging of the vitreous samples. Recently, Linkam has commercialized the setup, which raised the interest of multiple academic institutes. The first commercial setup has been installed in Birkbeck College, London, in the lab of professor Helen Saibil (figure 8).

Three major modifications were made to the stage (shown in figure 1). One of the modifications was aimed at improving the applicability of the specimen cartridge. The improved specimen cartridge is adapted to carry three grids at a time, which can be viewed with transmitted light through a coverslip of sapphire (figure 1A). The sapphire used has an improved thermal conductivity compared to the previously used brass, and a refractive index that allows transmitted light imaging such as bright field or phase contrast imaging (1.77; for comparison, the refractive index of glass is 1.5). In practice, the transmitted light imaging primarily facilitated finding focus, which is sometimes a challenge in FM mode when fluorescence signals are weak or rare, like in the case of vitreous sections. In addition, the transmitted light mode can be used to visualize where cells or sections are located (figure 8). Furthermore, the holder is surrounded by a brass rim to carry some liquid nitrogen during the first transfer into the stage, which ensures that the sample is kept cold for longer times during the specimen transfer. The liquid nitrogen will evaporate once the holder is inside the stage.

A second adaptation is an improvement aimed to reduce ice contamination. As illustrated in chapter 4, the setup regularly gave rise to ice contamination that was deposited on the sample during FM observations. The contamination consisted of small (~100 nm in diameter) ice crystals randomly spread over the grids, sometimes sparse, sometimes densely packed. In following experiments, most of this contamination proved to originate from the nitrogen gas that was used to purge the specimen chamber. When the gas flow was omitted during FM observations, the contamination surprisingly reduced. The nitrogen gas passed through silicon tubes from the nitrogen Dewar into the silver block, further into the nitrogen pump, and back again into the specimen chamber. On its way, the gas became contaminated by small ice crystals that were likely present inside the tubes. We solved this contamination by replacing the gas ‘recycling’ route with a direct tube connection from the nitrogen Dewar into the chamber (figure 1B). Passive evaporation of nitrogen gas was sufficient to create an overpressure of uncontaminated gas in the stage, and prevent humid air from diffusing in. This improvement brought the amount of contamination down considerably, and therefore significantly improved the success rate in getting high quality images from the device. Due to the overpressure, the option arose to change objectives during an experiment. The overpressure of nitrogen gas assures that no humid air will enter the specimen chamber. However, the objectives must be of the same diameter, in order to fit in the same Teflon ring collar.

A third adaptation was aimed to improve the user-friendliness of the specimen transfer box (figure 1C). The outer, Styrofoam box is made more robustly by precise machining. Importantly, the box can be closed air-shut by a tight lid on top, and a small lid that fits in the transfer-opening. This

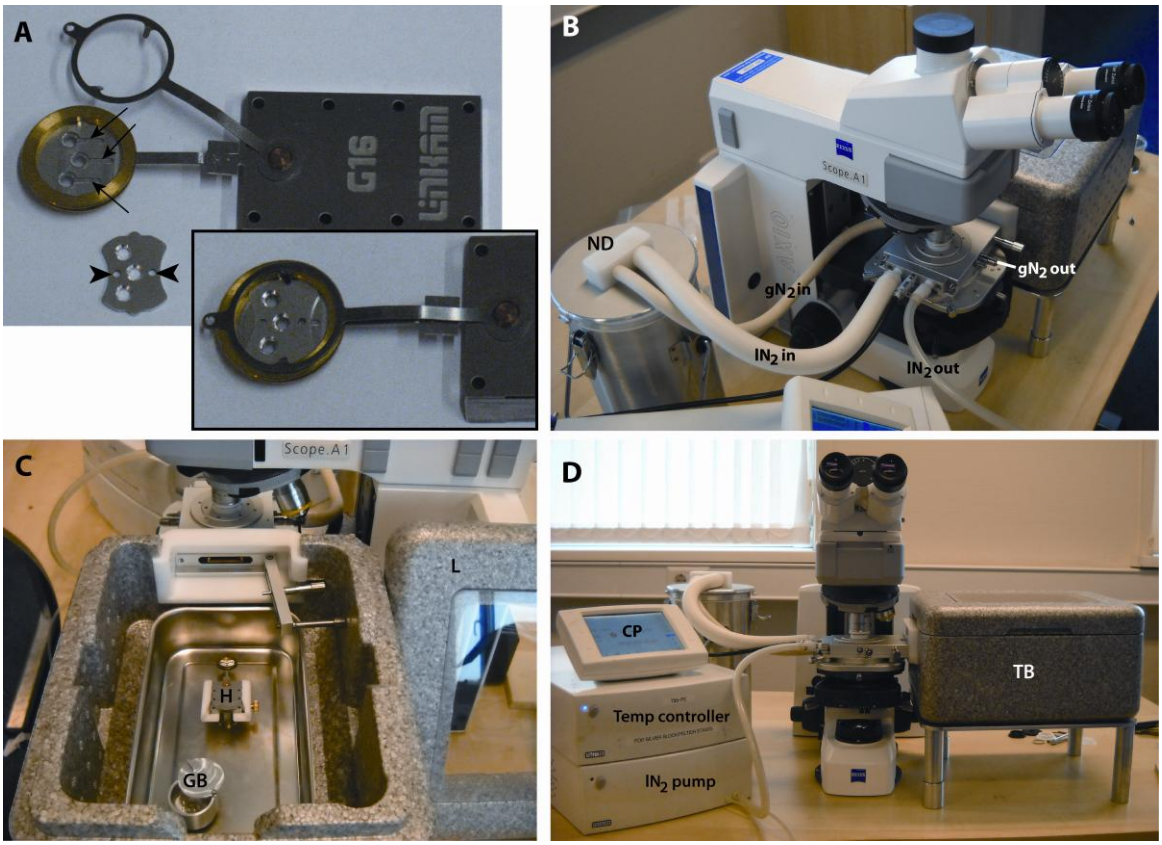

Figure 1. The second generation cryo-FM stage. (A) The sample loading cartridge consists of a body and a sample support element that lies on the cold silver block once inside the stage. The sample support element consist of several layers: a layer of sapphire with directly on top a layer of stainless steel with openings for three grids. The openings are at the end of elongated milled slots (arrows) that are made to grab the grids with a forceps from underneath. The next layer is a lid that presses the grids down once they are placed. The three openings in this lid also expose the grids, and the two smaller holes (arrowheads) are to transfer the lid with a forceps. The lid is finally clamped down by a sliding clamp that can be lifted and placed over the sample support element with a forceps. (B) The liquid nitrogen Dewar (ND) holds the nitrogen that is used to keep the silver block cold, and the specimen chamber dry. It has two outlets. One outlet is connected to a hose with thick insulating foam, through which liquid nitrogen is pumped to the silver block inside the stage (lN_2 in). The silver block supports the sample support element of the loading cartridge. The liquid nitrogen travels further out of the silver block (through the hose depicted as lN_2 out), into the nitrogen pump, from where it escapes as nitrogen gas. The second opening in the nitrogen Dewar leads the evaporating nitrogen gas via another insulated hose into the stage (gN_2 in). It builds up an overpressure of dry nitrogen gas in the stage, and can leave the stage through an outlet on the opposite side the stage (gN_2 out), or through an opening that may separate the objective lens and the Teflon collar. (C) Specimen transfer box. The box is made of Styrofoam, and comprises a solid plastic transfer opening, through which the sample loading cartridge can enter the stage. The top lid (L) and a smaller lid that fits in the transfer opening of the box together shut the box air-tight to prevent ice contamination while liquid nitrogen is kept inside. When shut, the inside of the box can be viewed through a plastic window in the top lid. Inside the Styrofoam box is a stainless steel bath where grids can be loaded into the sample loading cartridge under liquid nitrogen. It contains a compartment for a grid box (GB), and a compartment for the loading cartridge (H). (D) The total cryo-FM setup. The controlling devices to the left of the stage are the liquid nitrogen pump and the temperature controller. Both are controlled by the control panel (CP), which is a touch screen. On the touch screen, one can set the desired temperature of the silver block. The transfer box (TB) is placed on the side of the setup.

way, the box can be closed between transfers, while the liquid nitrogen remains inside for hours without getting contaminated by the influx of humid air. The lid of the box also contains a plastic window, so that the inside of the box is visible while it is shut, and the transfer-opening is made by a Teflon 'mouth piece' that fits exactly over the side-entry port of the cryo-stage. The inner, stainless steel box is left largely unchanged, with a compartment for a grid box and a Teflon holder that supports the specimen cartridge. The Teflon holder is slightly adapted to simplify the procedure of loading and unloading a specimen cartridge.

6.2.2. Cryo-ILEM

Alternatively to mounting a specialized cryo-stage on a light microscope setup is to integrate a light microscope into a TEM column. The development of an integrated light microscope in a TEM column was initiated in 2005 within the framework of a collaboration between Utrecht University (and later also the Leiden University Medical Center) together with FEI Company. The collaboration resulted in the ILEM (Agronskaia et al., 2008). The ILEM was initially developed for room temperature CLEM applications, but especially during the last few years it became clear that the setup would also be highly suitable for the imaging of vitreous samples. An integrated cryo-CLEM microscope circumvents possibly risky specimen transfers during which grids may become damaged or even get lost. An integrated microscope also allows for the use of incorporated software that can position a feature of interest in the two imaging modes with high accuracy.

The instrumental setup of the ILEM consists of three modules: a TEM, a laser scanning fluorescence microscope (LSFM), and a software module that unifies the two optical instruments (figure 2). The LSFM is inserted in the side-entry port of the TEM column opposing the objective aperture. To use the FM mode, the specimen holder must by tilted to 90°, at which angle the surface of the EM grid faces the objective lens of the LSFM. This position allows the LSFM to approach the specimen. The data shown in this chapter originate from two different ILEM setups that consist of a similar LSFM module, but considerably differ in TEM and software.

The TEM module of the cryo ILEM

Most of the data in this chapter originate from the ILEM set that was present at Utrecht University and consisted of an FEI Tecnai 12 Biotwin TEM operating at 120 kV. The electron source in this TEM was a tungsten filament, which has limited coherency and is therefore a less optimal electron source for cryo EM applications. Nevertheless, this ILEM setup was sufficient to show a proof of principal of cryo-ILEM. The latest data originate from a next prototype of the ILEM that was placed in the LUMC, and that is better equipped for cryo imaging. The TEM consists of an FEI Tecnai 12 Twin TEM which operates at 120 kV and is equipped with a LaB6 filament. The LaB6 source provides a more coherent electron beam, and is therefore better fit for cryo-EM than a tungsten gun. In this improved design of the ILEM, considerable safety measures were taken in

hardware and software to prevent possible damage of the microscope by incorrect use, and increase user friendliness. For example, only one slot of the objective lens aperture is available, which gives some restrictions to high contrast resin-embedded TEM (but not to cryo-EM). In addition, the aperture holder was shortened to provide sufficient space for the LSFM module between the upper and lower pole piece of the TEM objective lens. A further safety precaution is added to ensure that the aperture holder is retracted prior to switching to FM mode, so to prevent a pole touch (i.e. a mechanical touch between the EM objective lens and the FM objective lens). It consists of a sensor on the objective aperture control knob that is monitored by software in order to prevent the movement of the LSFM when the aperture is not yet set to the right position.

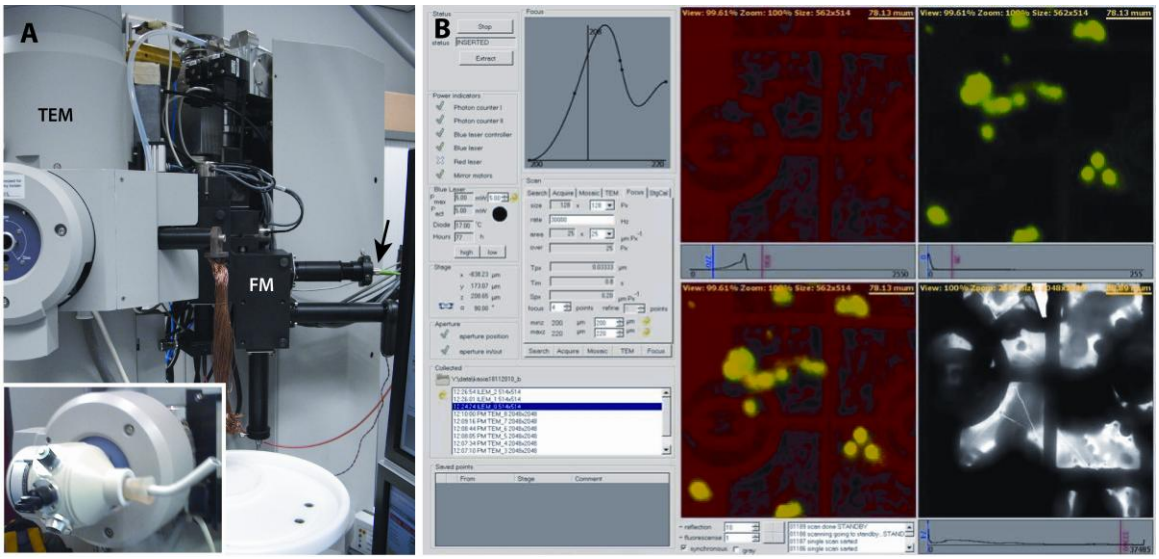

Figure 2. The integrated light and electron microscope (ILEM). (A) The LSFM is inserted in the side-entry port of the objective lens opposing the objective aperture. On the outside of the microscope, it is exposed (FM). It contains the lenses, laser insert and detectors. Inset: the cryo-EM holder is tilted to 90° to allow approaching of the FM module. To prevent the liquid nitrogen from pouring out of the Dewar at this angle, the opening of the Dewar was closed by a rubber cork containing an upward-facing outlet. (B) The software interface of the ILEM. The four main windows display the emitted fluorescence (upper left), the reflected laser light (upper right), the overlay of the fluorescence and reflection signals (lower left), and the EM image that can be taken independently in a corresponding area (lower right). To the left of the display windows are the adjustable parameters of the software. Options are to activate or deactivate the laser, set the laser power, set the field of view, scan speed and image output size of an image in a search, focus and exposure mode, perform automatic focusing, and take an automated FM image stitch. In addition, a browser shows the saved images, which can be loaded on request and displayed in the display windows. By clicking in the images, the coordinates can be saved for later imaging, or the stage can be directed immediately to the corresponding coordinates.

In both TEMs, the sample stages were modified to allow tilt angles from +90° to -70° (and -90° at the LUMC). When the sample holder is tilted to 90°, the retracted FM module can approach the sample from the side of the TEM column. A problem that we encountered when a cryo-holder was tilted to 90°, is that the liquid nitrogen in the holder Dewar poured out. We minimized this problem

by replacing the normal lid on the holder Dewar with a rubber cork containing an outlet that points upward (figure 2A). This construction allowed cryo-FM examination for about an hour, before having to refill the Dewar.

The FM module of the cryo ILEM

The LSFM is inserted in the side entry port of the objective lens opposing the TEM objective aperture. For vacuum compatibility, limited space and less electron optical aberrations, a single glass molded aspherical objective lens with a laser scanning geometry was used, having an NA of 0.55 and a working distance of 3.1 mm. This setup obtained a resolution of ~600 nm. For FM imaging, the electron beam is turned off, the specimen holder is tilted to 90°, and the LSFM moves toward the sample. Focusing is done by adjusting the Z-axis of the stage.

The FM module used to obtain the data presented in this chapter differs from the original published FM module in three aspects. Firstly, the 473 nm wavelength laser was replaced by a 488 nm laser, since this wavelength is more suitable for a number of widely used fluorophores. Second, an additional detector was added to the microscope. Whereas the original detector senses the fluorescence that is emitted from the sample upon laser illumination (fluorescence detector), this second detector is used to sense reflected excitation signals (reflection detector). The reflected signals mostly resulted from reflecting metal grid bars and aided in the visualization of the grid patterns. Interestingly, however, the reflected laser light also revealed line patterns in the sample which are not related to the metal specimen carrier, but to the sample itself. The patterns appeared as altitude lines, and seemed to correspond to an interference pattern that displayed differences in ice thickness (as was observed by subsequent TEM imaging). For instance, narrow altitude lines that are close together corresponded to the rapidly increasing thickness of a cell, whereas the parts that do not change thickness display lines much further apart (figure 3). Where the ice thickness was constant (i.e. cells are absent), the reflection signal showed a homogeneous distribution. Though we do not fully understand the exact quantitative nature of the patterns, they convey useful information on where cells are present, and give an indication of the ice thickness. This information aids in judging if areas observed in cryo-FM are also suitable for subsequent cryo-EM, where specimen thickness should be less than a few hundred nm.

Third, whereas the material that held the objective lens of the FM-module was originally constructed of stainless steel, this has been replaced by phosphor bronze. This material is non-magnetic, and therefore does not influence the charged electron beam. When the LSFM is retracted, the TEM mode can be operated as a normal microscope. We made sure that the optical properties of the TEM, especially related to astigmatism and attainable resolution, were not affected by the retracted LSFM. To do so, we imaged Thon diagrams on carbon film, both with a room-temperature holder and a cryo specimen-holder cooled down to liquid nitrogen temperature. We also confirmed that the cryo-EM performance was not affected by the presence of the LSFM.

For this purpose, we performed cryo electron tomography on mitochondria in plunge-frozen mouse embryonic fibroblasts.

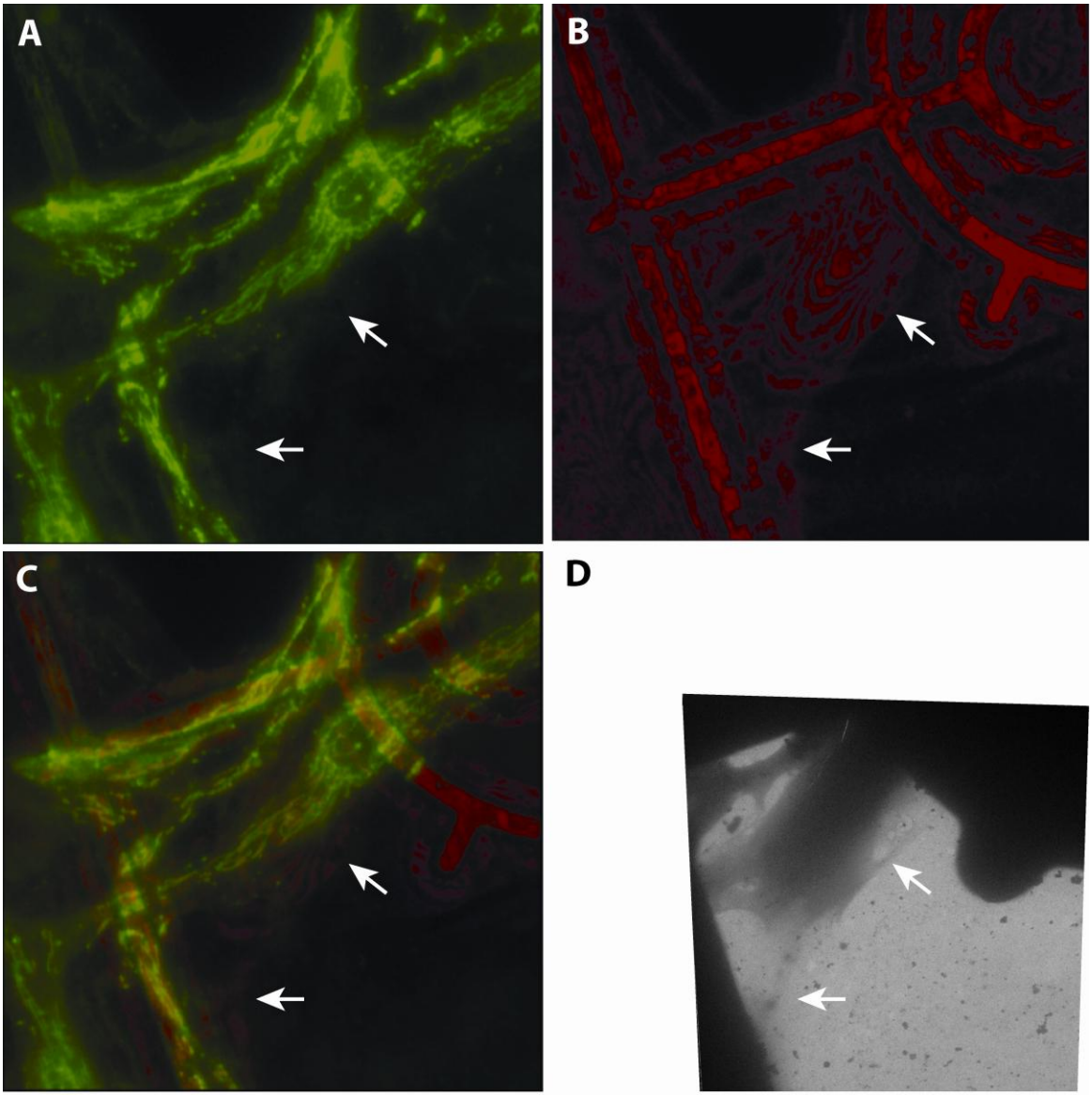

Figure 3. Reflected laser light of the ILEM shows grid bars and an 'altitude pattern' of the sample. (A) cryo-FM image of MEF cells labeled with mitotracker green. (B) Reflected laser light of the corresponding area in (A), that shows the grid bar patterns, and altitude lines in the area where a cell is located. (C) Overlay of the fluorescence light (A) and the reflected light (B) of the same area. (D) Low magnification EM image of the corresponding area in (A), (B), and (C). Notice that in locations where the thinnest remnants of the cell are located (arrows), a faint, broad altitude line was present in the reflected light signal, whereas in locations where the cell thickness quickly increases, the altitude lines became thinner and more closely spaced together.

The Software module of the cryo ILEM

The software of the original ILEM setup as present at the Utrecht University controls the actions of the FM module. The software user-interface has options to insert/retract the LSFM, move the X,Y,Z- and tilt angle motors of the goniometer, change the laser power up to a maximum of 20

mW, change the field of view (ranging from 800 x 800 µm to 10 x 10 µm), and change the format of the output images (ranging from 1024 x 1024 to 128 x 128 pixels). In addition, the software calculated the X/Y-coordinates that a specific spot in FM mode should have in TEM mode.

The software of the ILEM setup as present at the LUMC is aimed to fully integrate the TEM and FM modules and was completely rewritten compared to the Utrecht implementation. The XY-coordinates are linked and calibrated between the FM and TEM imaging modes. By interactively selecting areas in FM or TEM images in the software interface, the software will direct the stage to the corresponding coordinates in either imaging mode. The software interface (figure 2B) is improved to increase the user friendliness. It contains image display views that show the reflected light image, the emitted fluorescence image, the reflection-fluorescence overlay image, and a TEM image. Its functionalities for controlling the FM parameters are similar to the previous version, but supplemented with an auto-focus option and the possibility to automatically take FM image montages.

Data collection workflow

Although it is often reported that the electron beam quenches the fluorescence, it is also an option to start a cryo-CLEM experiment with a very low magnification TEM overview of an EM grid (figure 4A). The low magnification is required to keep the electron dose exposure of the specimen to the minimum. Such an overview gives an impression of the general state of the sample: variations in ice thickness and the presence of cells or other obvious structures such as broken meshes. When a sufficient low magnification and electron dose was used, the fluorescence signal is not visibly affected (figure 4B). The exact relation between the loss of fluorescence and electron dose exposure is yet to be measured, yet the tolerable dose will likely depend on the brightness and concentration of a fluorophore.

In FM-mode, the sample can be browsed in low magnification (e.g. over and area of 400x400 µm) specifically in the regions that revealed thin ice. In areas that show a potential region of interest, an automatic focus series is applied, and FM images are taken with a relatively low laser power, high scan speed and low image resolution (figure 5A). In these images, attention is paid to the reflection signal of the ice (figure 5B), to judge which regions of the sample seem to be best for taking high quality FM images. Areas are selected that appear acceptable for cryo-electron tomography in a later stage of the workflow (i.e. that are sufficiently thin). In these areas, high quality FM images are taken (i.e. with a higher laser power, a slow scan rate, and a good image resolution).

Following FM imaging, we switch to TEM mode, and direct the goniometer by selecting a potential region of interest in one of the FM images. TEM overview images, high quality images, and cryo-electron tomograms can finally be taken in these areas (figure 5D-G).

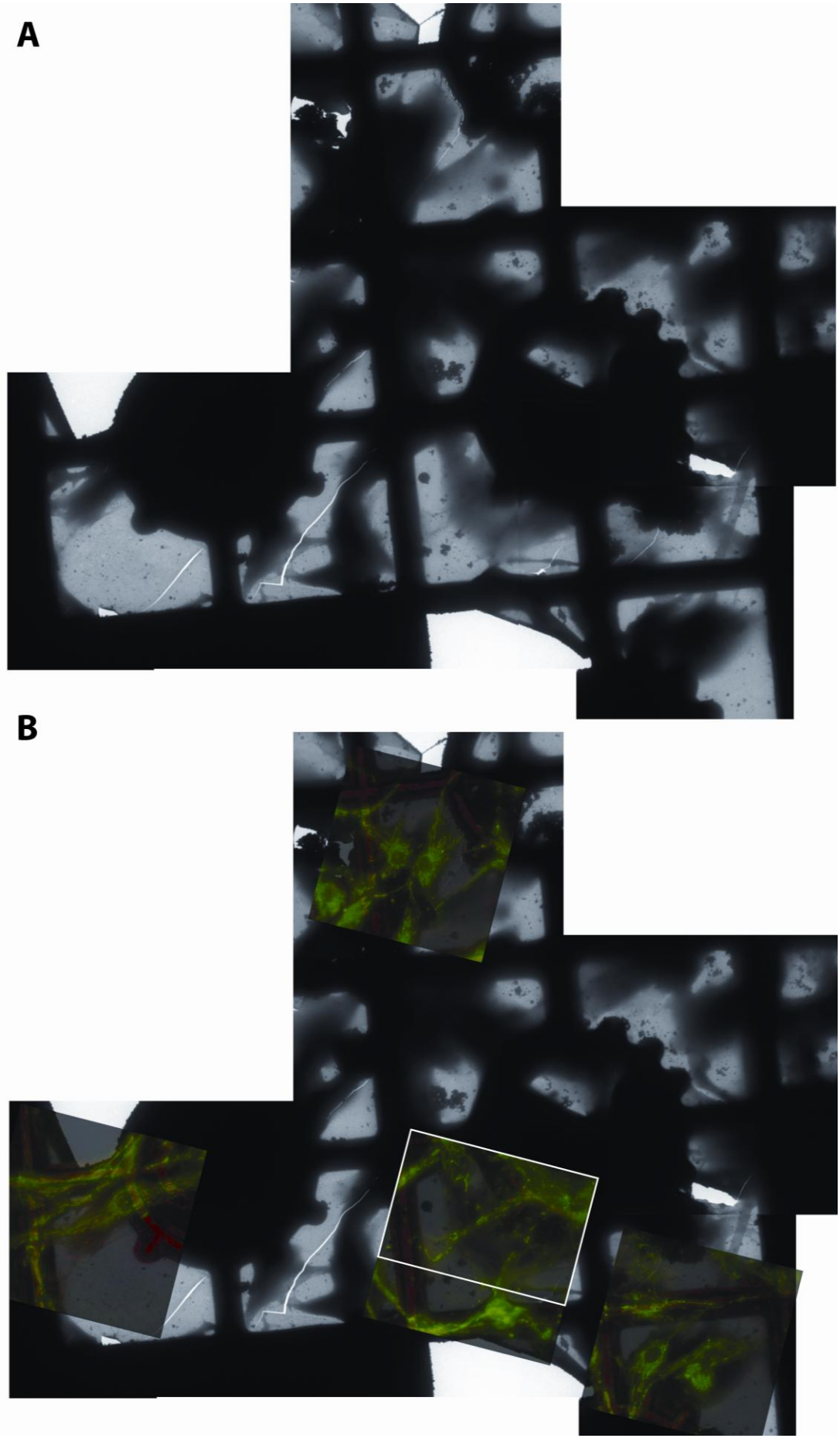
A
B

Figure 4. Low dose EM imaging does not quench FM signals. (A) Low magnification (~150 x) cryo-EM image stitch of a grid containing vitrified MEF cells labeled with mitotracker green. The overview reveals where cells are located, and which areas are likely to be thin enough for cryo-EM and cryo-electron tomography. In these areas, cryo-FM images were taken (B). The fluorescence in the sample is preserved, since a sufficiently low electron dose was used to perform the EM image stitch. The fluorescence preservation also applies to thin areas of the cells (see figure 5).

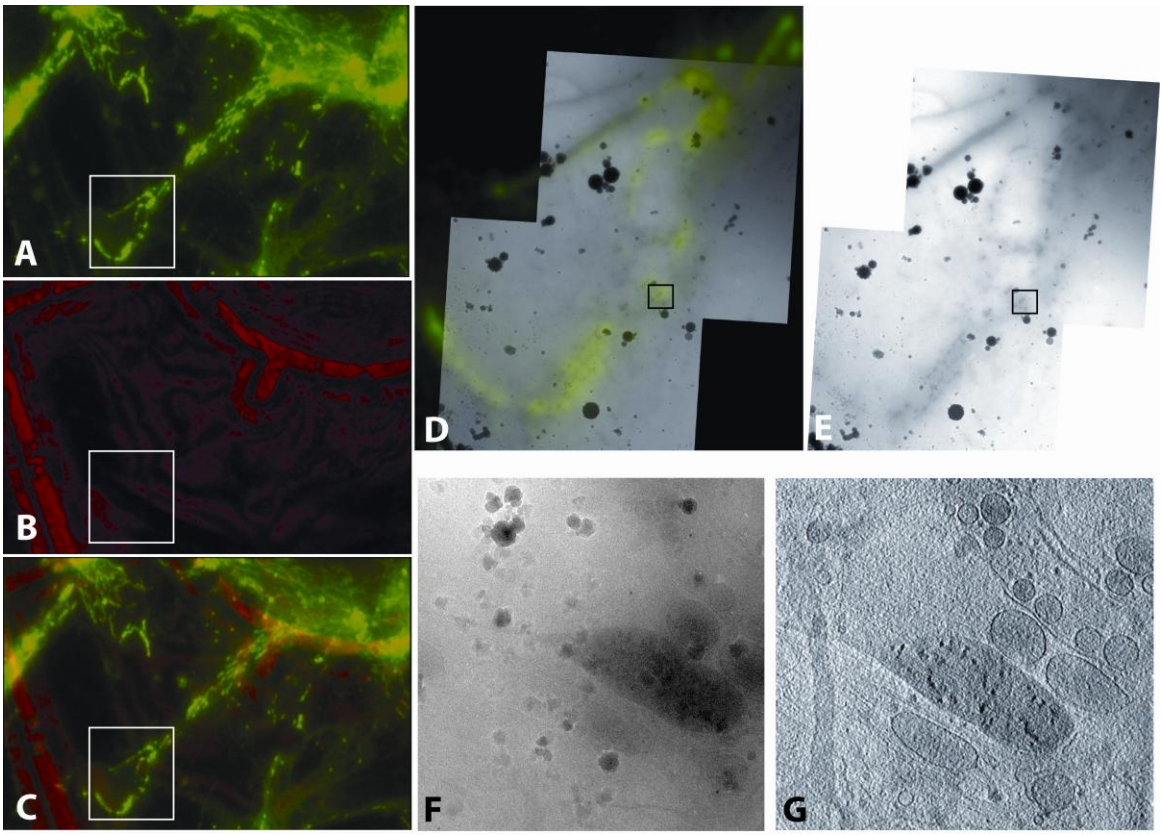

Figure 5. Sequence of images throughout the cryo-CLEM workflow in the ILEM. (A), (B) and (C) Fluorescence, reflection and overlay images, respectively, of the boxed area in figure 4B. (D) The corresponding EM image is superimposed onto the fluorescence area boxed in (A), (B) and (C). The EM image reveals electron densities in the locations where fluorescence is present (E), and mitochondria are thus located. (F) Higher magnification of one of the mitochondria (boxed area in (D) and (E)). Note that the image quality is rather poor due to the use of a tungsten filament in this TEM, which is not optimal for cryo-EM imaging. The cryo-electron tomogram of this area (G) already reveals much more detail.

6.3. Cutting Edge CLEM

Most CLEM techniques, like the ones described in this thesis, emerged during the last five years. Consequently, they are applied to only few biological systems. Their future development into mature CLEM techniques with a wide range of applications is dependent on 1) the quality of results they deliver, in terms of fluorescence and ultrastructural preservation, 2) the reliability that an EM structure exactly corresponds to the observed FM feature, and 3) the range of biological questions they are relevant to. Method improvements that will contribute to these factors are discussed below.

6.3.1. Automation

Important contributing factors to the success of EM techniques such as electron tomography, single particle EM and serial block face SEM, are the rapidly increasing possibilities and speed of automation and computing power. As holds for these EM techniques, the development and application of CLEM will thrive when it is combined with automation tools: automatic LM image stitches of complete grids, automated retrieval of structures of interest in EM, and automatic overlays of LM and EM views. A CLEM method that incorporates all these abilities in its software, as was pursued for the ILEM system, can therefore be very effective. But one can also think of other integrated instruments. For example, an instrument with separated FM and TEM devices, but which uses the same specimen holder and an integrated software system. Since such an approach avoids specimen transfers from one holder to another between imaging modes, it provides a mechanism for direct coordinate translation, while the advantages of a separate cryo-FM system is preserved.

A published example of automated CLEM is given by Vicidomini et al. (2008), who designed a procedure specifically for fluorescent labels in serial EM sections. Their software tool assembles 2D images from serial sections into 3D fluorescent structures, thereby positioning the corresponding EM images or tomograms in a 3D context. Advances in automation will make CLEM procedures easier and especially faster, and will therefore indirectly contribute to the value of the techniques. The advances would also create the option to combine CLEM with other high-end EM techniques, like FIB-SEM for plastic-embedded material and subtomogram averaging for frozen hydrated material. In fact, the first correlative FIB-SEM experiments have already been undertaken (Armer et al., 2009).

Positioning Accuracy

An important aspect of CLEM that can be greatly improved by automation is the accurate retrieval in TEM of a fluorescently labeled structure identified in FM. The positioning accuracy is important,

since structures of interest can be obscured in EM by superimposing structures in a section, or structures can simply have an unknown morphology. For cryo-CLEM, a precise positioning accuracy is even more crucial, since the amount of electron dose that can be used is much more restricted. On frozen-hydrated material, an electron tomogram can only be taken once at a feature of interest, and it is therefore crucial that the structure is indeed at the position indicated. In chapter 4, we describe a method for semi-automated retrieval of fluorescent features of interest in (cryo-)EM. What the program needs as a feed, are landmarks that can easily be observed by LM as well as TEM. In case LM and TEM are both performed on an EM grid, these landmarks can consist of grid bar corners. In other cases, landmarks may also consist of other fluorescent-electron dense markers that are added to the sample, or an organelle that is easily recognized in TEM may be fluorescently labeled. The program has a positioning accuracy in the order of 500 nm, which is comparable to the accuracy of the automated coordinate retrieval tool in the ILEM, and to another program described for cryo-CLEM procedures by Lucic et al. (2007).

For some applications, it would be beneficial to improve the positioning accuracy. In an ideal situation, one can record a tomographic tilt series based solely on the positioning software (i.e. without the need for visual inspection), and end up with the structure of interest nicely centered in the resulting tomogram. A high accuracy can be achieved by increasing the amount of landmarks used for the coordinate translation. This is possible by recording large grid overviews of every new grid, to incorporate enough landmarks. However, and especially when dealing with (vitreous) sections, local distortions in a sample that arise due to exposure to the electron beam will influence the position of features of interest in unpredictable ways, and thereby cause inaccurate positioning. A practical approach to circumvent this is to deliberately position a large amount of landmarks that are spaced closer together around a structure of interest. Kukulski et al. (2011) elegantly show that this strategy can greatly improve positioning accuracy. Fluorescent/ electron dense beads were adhered to a grid, and used as landmarks in a software script very similar to the one described in chapter 4. The script calculates the transformations between FM and TEM coordinates, to predict the TEM coordinates of the fluorescent feature of interest. The method was shown to pinpoint a fluorescently labeled structure in a resin section with an accuracy better than 100 nm. Such accuracy circumvents the need for a visual search, and indeed enables one to take a tomogram blindly. The method should also be suitable for cryo-CLEM approaches. In this case, the beads are adhered to a bear grid before a sample is added, or included in a watery solution before vitrification. In the case of the ILEM, the automated coordinate translation implemented in the software would need to be extended with an additional step of positioning refinement.

6.3.2. Optical Resolution

It is sometimes argued that a good optical resolution is not required in CLEM, since TEM will provide the high resolution information. However, this statement holds only in few cases. For

example, when the goal of the FM step is simply to discern transfected from non-transfected cells, or when large organelles are labeled. However, to discern smaller structures like microtubules or macromolecular complexes, a better optical resolution is required. In addition, it is in some cases important to visualize the shape of a structure, something that also requires a resolution that provides sufficient detail. This was the case for the WGA-alexa stained goblet cells in chapter 2, where the shape of the mucus granule compartment revealed whether the Golgi area was present in the section. Also in chapter 5, where the actin coated granules could be discerned from other actin patches by their characteristic ring-shape. The rings had a diameter of 800 nm ± 200 nm. With a lateral resolution of 400 nm, the cryo-FM stage was capable of visualizing clear actin rings, including the smaller versions (figure 6).

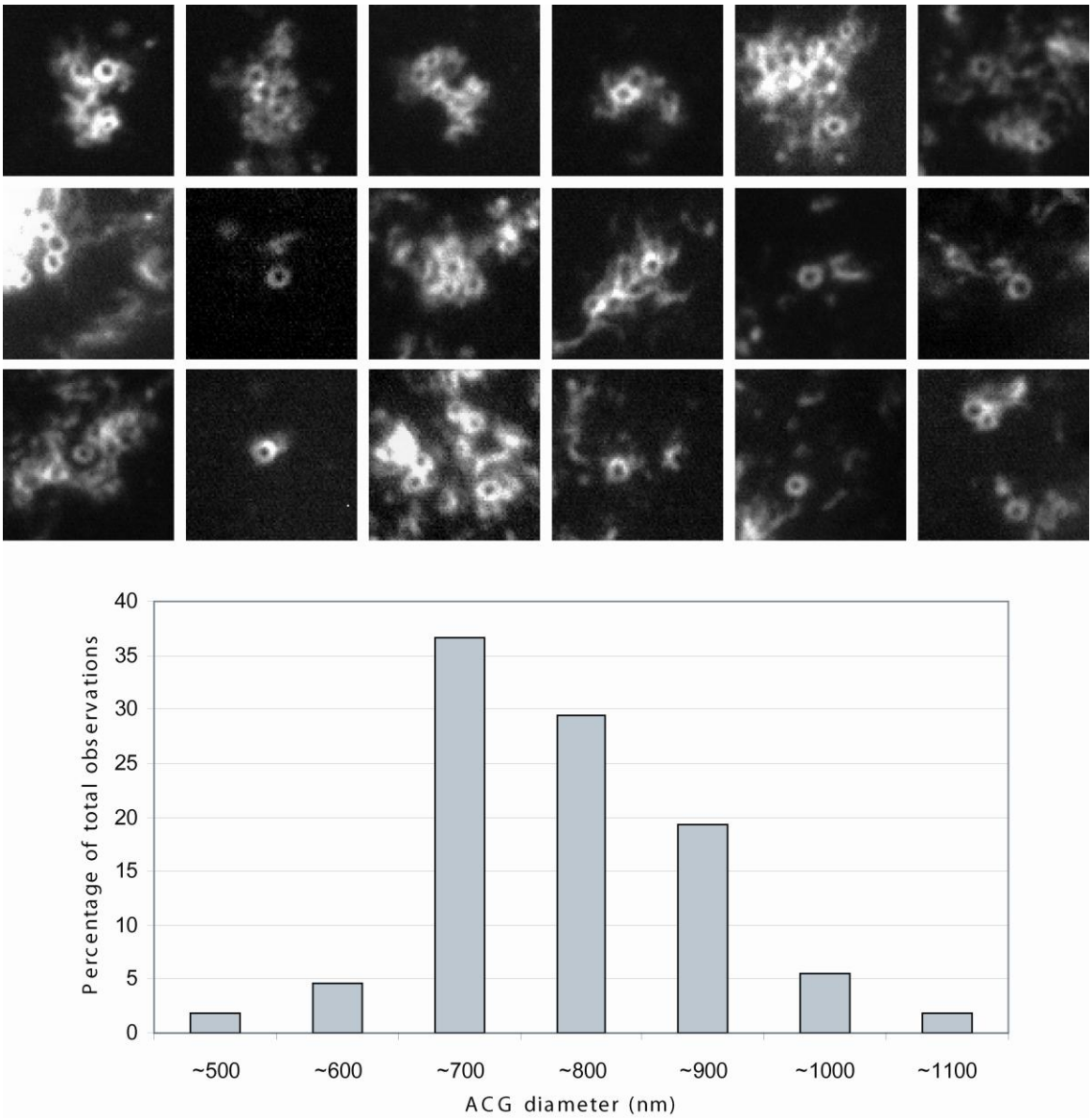

Figure 6. Actin coats display a range of diameters. Filamentous actin was labeled in pancreatic tissue homogenates with phalloidin-alexa 488 and imaged in cryo-FM (see chapter 5). (A) Different sizes of actin coats. Boxes are 10 x 10 µm in size. (B) Distribution of actin coat diameters as observed in 110 actin coats imaged over five different experiments.

Generally, when a structure of interest is too small to be distinguished by any type of LM technique, studies pursue a CLEM technique where an FM signal can accompany an electron dense marker. In this case, the FM label can give a broad positioning of the structure and the EM label an exact localization. Methods for this are described in chapter 1. Though the combined LM-EM markers approach is very powerful, it has some limitations. A major limitation is that the bifunctional probes are in most cases membrane impermeable, and their use is therefore restricted to the study of extracellular targets, or to the immuno-localization of targets on embedded TEM-section. An alternative approach is to photooxidate diaminobenzidine (DAB). This approach is easier to apply to intracellular targets, but requires chemical fixation of the sample, is not suitable for all types of fluorophores, and results in a rather poor spatial resolution of the deposited reaction product.

Novel attempts are made to design CLEM markers that overcome these limitations. For example the development of the fluorescent protein mini-SOG, which can photooxidate DAB more efficiently than GFP into the electron dense precipitate (Shu et al., 2011). A promising, recent development that is also applicable to cryo-immobilization, is the production of a genetically encoded fusion protein of GFP and ferritin (Wang et al., 2011). The probe combination is fluorescent by the GFP, whereas the ferritin becomes loaded with electron dense iron particles when they are supplemented in the culture medium. The authors used FM and cryo-electron tomography to show that the probe correctly localizes in E. coli cells when conjugated to several different proteins. The probe is therefore a promising localization tool, that can likely also be used for room temperature CLEM applications. Nevertheless, it should be noted that a drawback of any kind of electron dense marker is that it can obstruct the view of the ultrastructural detail in the labeled locations.

Optical resolution in cryo-FM

The diffraction-based resolution limit is given by $r = (0.61\lambda) /NA$, where r is the resolution limit, λ is the wavelength of light used for the excitation, and NA the numerical aperture of the objective lens. The optical resolution can therefore mostly be influenced by the NA. Currently, high NA objective lenses cannot be used in combination with cryo-FM, since these lenses demand a short working distance and preferably an immersion fluid. Both of these requirements are incompatible with vitreous samples, leaving the resolution for cryo-FM limited by the NA of long working distance, dry objective lenses. The highest NA of lenses that have been used in combination with cryo-FM stages is 0.75 (chapter 4; Rigort et al., 2010), which yield a theoretical resolution limit of ~400 nm.

We verified this limit in the cryo-FM stage by direct measurement of the point spread function (chapter four). The lens of the FM module in the ILEM has an NA of 0.55 and working distance of 3.1 mm, and can reach a resolution of ~600 nm (Agronskaia et al., 2008). To illustrate the lateral resolving power of the cryo-FM stage and the ILEM, figure 7 shows fluorescent mitochondria in

MEF cells, in vitro grown fluorescent microtubules, and microtubule plus-end binding proteins that were imaged in either of the setups.

When better resolutions are needed than the 400 nm of the cryo-FM stage, one approach is to perform FM imaging prior to vitrification and cryo-EM. In this way, cells are settled on EM grids, and imaging can be performed on a typical FM instrument using high NA oil-immersion lenses. However, this workflow often requires that cells or structures are lightly fixed to prevent them from moving. And even fixation cannot prevent that cells occasionally detach from the grids or change location, thereby making retrieval of the same structures complicated (Briegel et al., 2010). Also the procedure that is required for plunge-freezing (e.g. blotting and plunging) can alter the appearance and localization of cells (Lepper et al., 2010).

For future developments, there are several possibilities to improve the resolution of cryo-FM. One important option is to extend the types of suitable objective lenses with higher NA objective lenses, i.e. with a short working distance and with an immersion fluid. This would require that the objective is prevented from warming up the specimen. It might be possible to cool the objective from above down to the devitrification temperature (-140˚C). Though future experiments have to give a decisive answer, preliminary experiments indicate that the repeated dipping of regular objective lenses into a bath of liquid nitrogen over extended periods maintains the integrity and performance of the lenses (Le Gros et al., 2009). This latter study gives another interesting possibility: the use of a cryogenic immersion fluid. The authors used liquid propane or isopentane, both of which are liquid at liquid nitrogen temperatures, and have a refractive index close to that of water. Theoretically therefore, water-immersion lenses in combination with a cryogenic immersion fluid could yield the same resolution as water-immersion lenses in combination with water.

Super-resolution FM

A way to bring the resolving power of FM, and perhaps also of cryo-FM, to a level beyond the diffraction limit would be in the footsteps of super-resolution FM techniques (Patterson et al., 2010). Super-resolution FM is a recent development that is gaining in momentum in the imaging world. One of the first techniques, stimulated emission depletion (STED) microscopy, is based on a confocal setup, in which the excitation beam is overlapped with a doughnut-shaped beam that is capable of de-exciting fluorophores by emission depletion (Hell and Wichmann, 1994). The precise alignment of the two beams ensures that fluorescence is allowed only in the central area of the excitation spot where the doughnut beam is near zero. Scanning with such a narrowed spot across the sample yielded images with a resolution that for the first time broke the diffraction barrier of light: around 50 nm (Hell, 2003; Willig et al., 2006). Later, techniques arose that again improve this resolution range, like PALM (photo-activated localization microscopy) and STORM (stochastic optical reconstruction microscopy) (Betzig et al., 2006; Rust et al., 2006). They use total internal reflection (TIRF) or wide field illumination to selectively detect individual

photoactivatable or photoswitchable fluorophore molecules. Many images of randomly switched-on fluorophores are summed up to create a 2D image with a resolution around 10 nm.

When amenable with CLEM, super-resolution FM will extend the possible applications with smaller and more densely distributed cellular structures. Super-resolution FM techniques have already been used in conjunction with room temperature CLEM methods. PALM was shown to be feasible on Tokuyasu sections (Betzig et al., 2006), and a recent publication gave the first promising results of STED and PALM microscopy in ultrathin resin sections (Watanabe et al., 2010).

It would be interesting to see whether these super-resolution techniques can be combined with cryo-FM. Clearly, the combination would render cryo-CLEM suitable for smaller structures, and the positioning accuracy in EM more exact due to the more precise localization of reference points. However, cryo-FM also has the potential to improve the performance of the super-resolution techniques themselves. First of all, vitrification is a non-invasive fixation method that leaves the high resolution details of cells unaltered. This is in contrast to chemical fixation, which is known to cause artifacts. Although the artifacts do not disturb low resolution images from conventional light microscopes, the super-resolution microscopes will resolve them, and they can cause problems in image analysis. Secondly, cryo-FM has the potential to further improve the achievable resolution of super-resolution techniques. At cryogenic temperatures, fluorophores have a higher fluorescence yield due to the strongly reduced rate of photobleaching (Schwartz et al., 2007; see also the section 'Fluorophores in cryo-FM'). This means that the number of photons detected per molecule, before it photobleaches or reverts to a dark state, increases, and the lateral position coordinates can be determined more accurately (Betzig et al., 2006; Hell, 2003; Thompson et al., 2002). A requirement that currently prevents super-resolution FM techniques to be applicable at cryogenic temperatures is that the systems use high NA, oil-immersion objective lenses. The progress described earlier on cryogenic immersion fluids thus represents the first step towards super-resolution cryo-FM and cryo-CLEM.

Figure 7. Comparison of the image quality of the ILEM [(A), (B) and (C)] and cryo-FM stage [(A'), (B') and (C')]. (A/A'/A'') show cells in which the mitochondria have been labeled. Insets are 10 µm by 10 µm. Mitochondria are clearly seen in EM, since they are relatively large organelles with a characteristic ultrastructure (A''). This cryo-EM image was taken after cryo-FM in an FEI Tecnai 20 at 200 kV. The corresponding cryo-FM image is, however, not shown. In (B/B'/B''), microtubules have polymerized from tubulin dimers conjugated to Hilyte-488. Insets are 10 µm by 10 µm. The cryo-EM image (B'') was taken in the ILEM, and corresponds to the boxed region in (B). In (C/C'/C''), microtubule plus-ends in neuroblastoma cells (C) and MEF cells (C') were labeled with the plus-end binding protein CLIP-170 conjugated to GFP. The cell nuclei (N) are prominent, because the fluorescence in the thicker regions of the cells is scattered by the thick ice. The scattering causes difficulties to discern the faint plus-end signals from the background fluorescence. In the thin cell process extending from the neuroblastoma cell (arrow in (C)) the plus ends are more easily recognized. The EM image is taken in the periphery of the cell displayed in (C'), and was taken in the same microscope as (A''). Besides other cellular structures, several microtubules can be observed (arrows). Scale bars represent 10 µm in (A), 200 nm in (A''), 10 µm in (B), 100 nm in (B''), 10 µm in (C), and 200 nm in (C'').

The impressive resolution that current super-resolution FM techniques can achieve sometimes calls for the question whether these techniques don't make EM techniques, including CLEM, superfluous techniques. However, the two types of microscopy are actually complementary. The most characteristic feature of FM is that it images fluorescent labels. The labels can accompany only one or several structures per experiment, since the emission wavelengths of their respective fluorophores need to be discerned. In addition, not all proteins have the option to be labeled, and sometimes the labels interfere with the physiological functioning of proteins. When the function of a protein is studied in relation to other structures, extensive prior knowledge is necessary to

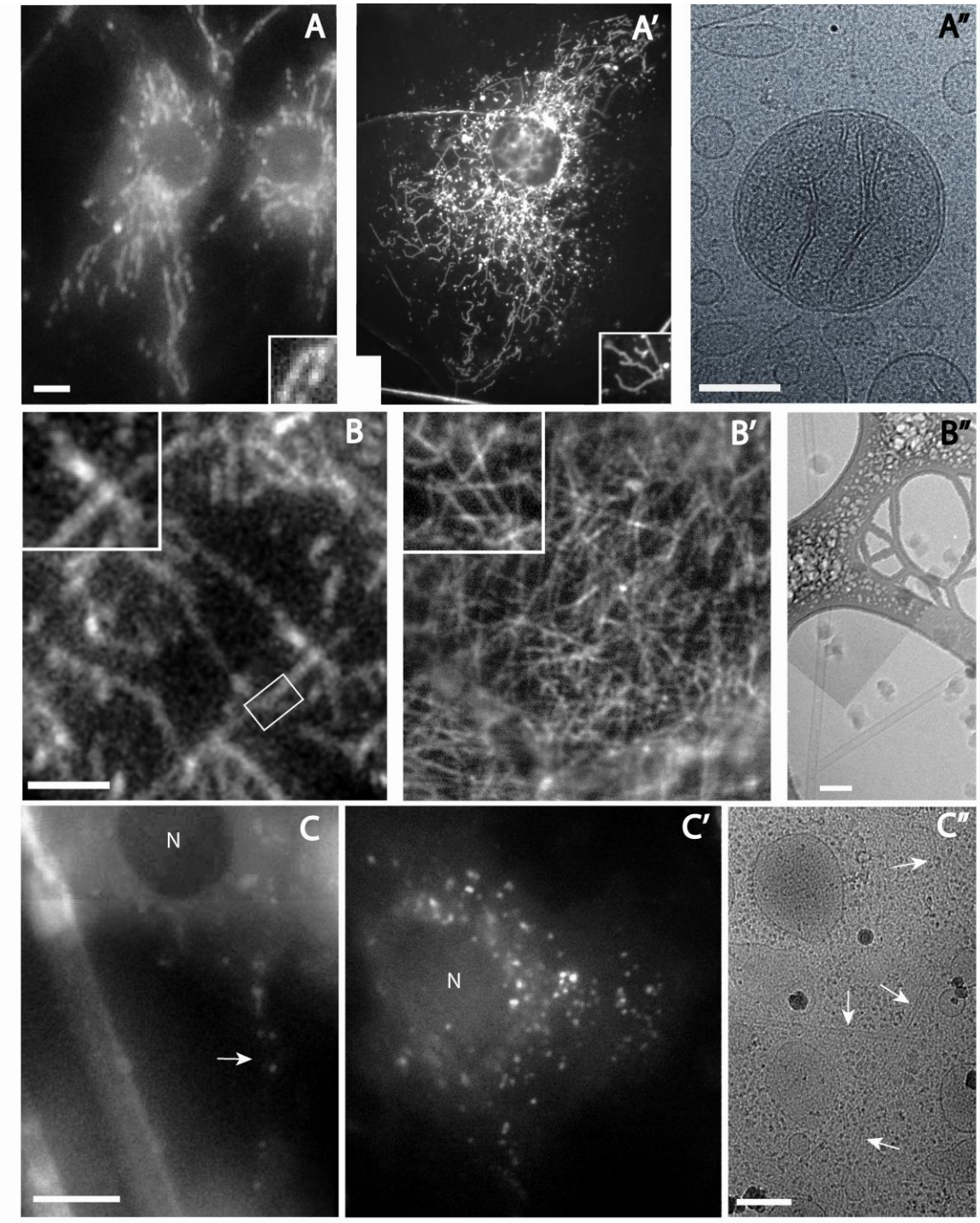

assign potential interaction candidates. EM, on the other hand, images mass densities that are independent of specific labels. Although this trait facilitates an unprejudiced view of samples, it can also render images difficult to interpret. Combined, super-resolution FM and EM will provide both high resolution functional and ultrastructural information.

6.3.3. Sensitivity of FM methods in CLEM

The structures that are studied in EM are generally small, such as viruses, protein complexes and microtubules, and can therefore be labeled with only a limited amount of fluorophores. In the case of immunolabeling techniques, a further restriction is that not all of the epitopes are within reach of the antibodies, making signals even weaker (chapter two). It is therefore important that CLEM preparation methods preserve fluorescence signals as optimally as possible. For room temperature CLEM applications, the preparation techniques for EM often proceed at the expense of fluorescence intensity, keeping it out of reach for some applications. Sims and Hardin (2006; 2007) and Nixon et al (2009) provided the first promising results that high pressure freezing followed by a slightly adapted freeze substitution protocol preserves the fluorescence of GFP, RFP and rhodamine-phalloidin even in thin sections. Kukulski et al. (Kukulski et al., 2011) further adapted the protocol of Nixon et al. and demonstrated that their method results in a fluorescence intensity that is very similar to the intensity imaged by live cell imaging. One sacrifice that has to be made in the above protocols is that EM stains largely need to be omitted from the substitution medium. EM stains employ electron-dense heavy atoms (osmium, uranium, and lead compounds), which quench fluorescence. The most severe quenching effect is caused by the lipid-binding stain osmium tetroxide. Only when using bright signals, a compromise can be made between fluorescence preservation and a tiny amount of osmium (Watanabe et al., 2010).

An advantage of cryo-FM that should be noted is the reduced photobleaching that was mentioned earlier. This means that, if exposure times are long enough, signals with a low photon emission flux can eventually integrate to give a good signal-to-noise ratio. Nevertheless, other factors also contribute to the sensitivity of a cryo-fluorescence setup. First, the sensitivity, as for the resolution, depends on the NA of the objective lens. By definition, the NA depends on the half-angle of the objective's light collection cone (Inoue and Spring, 1997), meaning that higher NA lenses have the ability to collect more light. Second, the sensitivity depends on the characteristics of the detector used. The best mainstream detectors for epi-fluorescence microscopy, also at cryo temperatures, are cooled CCD cameras. These have a high photon detection efficiency (PDE), which means that a high percentage of the photons that fall on the detector are actually detected and transferred into a signal. In addition, readout noise levels are relatively low, and the image can be accumulated on the chip for a long time (Aikens et al., 1989). New advances in detector types for widefield FM are the EMCCD and scientific-grade CMOS cameras, which both exhibit a drastically improved sensitivity to fluorescence signals. In the case of laser scanning FM as in the

ILEM, photodiodes, and especially avalanche photodiodes, have a higher PDE than photomultipliers (~65%, respectively ~20%). Nevertheless, both photomultipliers and photodiodes provide the possibility to sum multiple images together to increase the signal-to-noise ratio.

In our cryo-FM setup, we use a 0.75 NA lens and a Leica CDD camera type DFC 350FX, which is cooled by a Peltier element. The ILEM uses a 0.55 NA lens combined with an avalanche photodiode detector. Both instruments were able to visualize fluorescence in ultrathin vitreous sections (figure 8) and fluorescent microtubules (figure 7B and B'). The in vitro microtubules consist of a mixture of tubulin and tubulin-Hilyte488, where, according to the manufacturer, the fluorochrome is bound to every one or two tubulin dimers. Taking the average of 0.75 fluorochromes per dimer, and given that a microtubule consists of 13 protofilaments and that a tubulin dimer is 8 nm in length, this is calculated to 1.2 Hilyte molecules per nanometer of a microtubule. But we could also detect weaker signals deriving from GFP-tagged EB3, a microtubule plus-end tracking protein that only binds to the growing ends of microtubules (figure 7C and C').

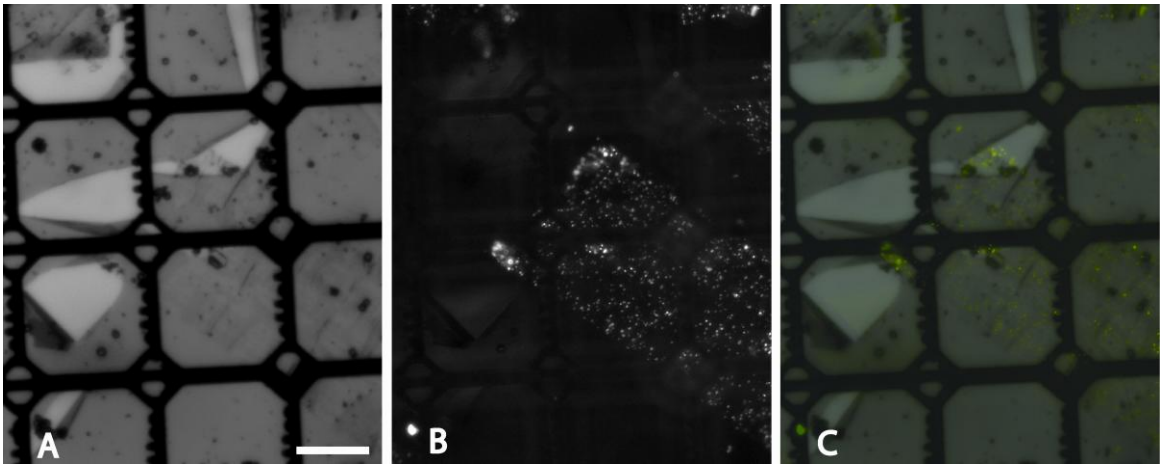

Figure 8. 70-nm vitreous sections containing yeast cells that express cytoplasmically located YFP. (A), (B) and (C) are transmitted light, fluorescence and overlay images, respectively. The transmitted light option was used to find focus and locate the position of the sections. These images were kindly provided by prof. Helen Saibil and Daniel Clare, from Birkbeck University, London, UK. Scale bar represents 100 µm.

6.3.4. Fluorophores in cryo-FM

When first starting up cryo-FM developments, it was unclear whether fluorophores would still fluoresce when embedded in vitrified ice. Several findings from studies in single molecule optics however indicated that this would be the case. In these studies, cryo conditions are often applied to study the electronic properties of molecules. The molecules are diluted in cryo-protectants like

glycerol, and kept in a cryostat at liquid helium temperatures by evaporating liquid helium. The low temperatures hamper most dynamic processes, while the chemical processes involving charge movements remain as active as at room temperature (Hoffmann et al., 2008). Thus, the low temperatures allow these studies to focus on isolated charge reactions, such as the jumping of negatively charged electrons to and from an excited state in fluorophores. For several dye molecules, it was found that, whereas excitation at room temperature elicited large rearrangements of charge distributions, at cryogenic temperatures the geometrical changes were only very small (Moerner and Orrit, 1999). Accordingly, the absorption and fluorescence spectra of the molecules were narrower than at room temperature. The fluorescence is nevertheless retained. Another outcome of these studies was that the total number of photons that a molecule can emit is increased at low temperatures (Moerner and Orrit, 1999; Orrit, 2002). At ambient conditions, the fluorescence per molecule is limited to roughly 10^6 photons due to photobleaching, since the excitation can elicit chemical reactions with small reactive molecules such as oxygen and water that irreversibly damage the chemical structure of the fluorophore. At cryogenic temperatures, the reactive molecules cannot diffuse, and the structure of the fluorophore is preserved through more excitation cycles.

The current studies of cryo-FM of vitreous samples confirm most of the previous work in single-molecule optics: at liquid nitrogen temperatures, most fluorophores retain their fluorescence, and photobleaching is strongly reduced. The fluorescent molecules used in cryo-FM experiments until now are: (e)GFP, YFP, alexa 488, alexa 568, Hylite488, the mitochondrial dye mitotracker, the calcium chelator Fura-2 AM, and the nucleic acid dyes SYTO 59, Sytox orange and Hoechst (chapter 4; Gruska et al., 2008; Le Gros et al., 2009; Lepper et al., 2010; Sartori et al., 2007; Schwartz et al., 2007). For one puzzling fluorophore, mCherry, fluorescence emission can no longer be detected after vitrifications (unpublished data; personal communication with Ariane Briegel). The reason for this is as yet unknown, but it might indicate that there are other molecules that exhibit the same phenomenon. Besides completely losing its fluorescence, it is also possible that, due to the immobilization of the molecule, the excitation and emission spectra changed beyond the filter settings used. However, the shift would need to cover tens of nanometers, since broad bandpass filters were used for the mCherry detection. For the future, it would be useful to characterize the behavior of fluorophores in cryo-FM in more detail. Important classes of fluorophores that have not been experimented on in cryo-FM, are photo-activatable and photo-switchable dyes. These would be necessary to undertake super-resolution cryo-FM experiments using PALM or STORM techniques. However, these fluorophores have been shown to be stable through freeze substitution and resin embedding (Watanabe et al., 2010), which gives us a first indication to believe that vitrification will also leave them active.

6.4. Conclusions

The increasing amount of literature discussing and using CLEM, including the CLEM techniques discussed in this thesis does not leave much need for speculation: CLEM has acquired a central role in many EM laboratories worldwide. The amount of variations in techniques has outnumbered the amount of EM preparation techniques alone, and is still growing.

Owing to the different biological questions assessed in CLEM, all the current methodologies complement, rather than compete with, each other. For example, cell cultures offer a controlled experimental environment and easy genetic modifications to incorporate genetic markers, whereas tissue samples represent a more physiological situation; LM visualization of complete, unsectioned samples contain more information in an overview, whereas LM observation in EM sections allow a direct correlation with EM; proteins labeled with a genetic fluorescent tag can be transiently expressed and imaged in live cells, whereas immunolabels detect endogenous, wildtype proteins; and so on. Nevertheless, some considerations in the design of a CLEM experiment are still based on the ease or the maturity of the application. Most prominently, chemical fixation is easier and more accessible than vitrification, and CLEM provides more matured techniques in comparison with cryo-CLEM workflows. The complexity of both the cryo alternatives often drives researchers to use their easier room temperature counterparts, although the improved preservation of ultrastructure as well as fluorescence does render them superior. It is therefore crucial for the quality of CLEM results that the cryo-techniques become easier, more accessible, and less time-demanding. The techniques and developments described in this chapter will contribute to that progress.

The two cryo-CLEM methods described and compared in this chapter both have their advantages and disadvantages, and can be preferred, depending on the biological application. The cryo- FM stage has a superior resolution to the current FM module in the ILEM. Furthermore, the stage can be implemented easily on any upright light microscope, works in conjunction with any kind of electron microscope, and is relatively low-cost. The visual scanning of multiple samples is also fairly quick, since three samples can be transferred at once, and since imaging with epi-fluorescence is generally much faster than imaging with laser scanning fluorescence microscopes as in the ILEM. Although the ILEM functions less in these mentioned categories, it can compensate greatly by its user friendliness. In this microscope, it is no longer necessary to manually transfer delicate vitreous samples from one microscope to another. In addition, the software and lateral coordinates of the two imaging modes are fully integrated, which also circumvents the step of coordinate retrieval, and provides the option for automatic LM and EM overlays. An unexpected advantage of the ILEM was that the reflected light images display a relative height profile of the sample, which indicates which areas are thinnest and best suitable for cryo-EM. Lastly, the device allows the multiple switching between imaging modes. Although one

has to consider that substantial electron dose will quench the fluorescence, low magnification TEM overviews can be made before switching to FM mode. Or, small areas of the sample can be imaged at high EM magnification, while the fluorescence in the rest of the sample remains intact.

Using the two methods, we found that the suitable fluorophores and the sensitivity of the cryo-CLEM techniques allow a wide variety of biological applications, including labels in ultrathin vitreous sections and GFP-tagged microtubule plus-end binding proteins that occupy no more than 30 nm^3. Instead, the applicable samples for cryo-CLEM are currently limited by the optical resolution of cryo-FM and the positioning accuracy of the retrieval software. A variety of advances can, however, improve both of these parameters in the future, such as cryogenic immersion fluids for the optical resolution, and the reduced spacing of reference points for the positioning accuracy. Note that improvements in resolution will, most likely, be applied more easily to the cryo-FM stage than to the ILEM, since the FM module in the ILEM operates under vacuum.

In the current phase of development, the complete cryo-CLEM workflow can be fulfilled within a day work, or, if tomography is included, an extra day may be required. This time-line is quite reproducible. A greater bottleneck than the technical workflow, in our experience, is the sample preparation, which can deliver samples of inconsistent quality in the case of plunge-freezing, and can be laborious and technically challenging in the case of HPF followed by vitreous sectioning. An improved cryo-CLEM method should therefore also assess these preparatory steps. Especially the sectioning of frozen-hydrated material may be improved by methods that reduce compression artifacts, or by developing alternative methods that are easier and more reliable. A promising option is for example focused ion beam milling (Hayles et al., 2010; Marko et al., 2007; Rigort et al., 2010), where a sample can be thinned to allow cryo-EM, or, ultimately, can cut ultrathin vitreous sections from a high pressure frozen sample.

6.5. Outlook

When all the improvements mentioned in this chapter can be applied to the current CLEM methods, the ultimate CLEM technique is a fully automated method that can detect weak fluorescence signals (e.g. arising from a single macromolecular complex), and localize them with high FM resolution, to subsequently position them in TEM with an accuracy that exceeds 100 nm. An addition to the FM techniques that would enrich its possibilities would be the addition of functional FM techniques like FRET analysis. FRET is used to study the interaction between two proteins, but can interestingly also be used to visualize intramolecular conformational changes (Truong and Ikura, 2001). Thus, a protein can be searched for that is in a particular conformational and thus functional state. Besides interesting for cellular biological studies, the latter option may be a method for single-particle analysis of proteins that exhibit different conformational states within a sample. Alternative to intramolecular FRET would also be fluorescent probes that fluoresce at different wavelengths dependent on the conformational state of a labeled protein (Cohen et al., 2005).

Despite of all the improvements in cryo methods, the equipment and skills necessary to complete a cryo-CLEM experiment will keep it a technique that is less accessible than room temperature techniques. For a long period to come, room temperature CLEM techniques will therefore remain the mainstream workflow, although enforced by vitrification methods, and cryo-CLEM will be its homologue for the biological applications that demand high resolution ultrastructural analysis.

References

Agronskaia, A.V., J.A. Valentijn, L.F. van Driel, C.T. Schneijdenberg, B.M. Humbel, P.M. van Bergen en Henegouwen, A.J. Verkleij, A.J. Koster, and H.C. Gerritsen, 2008. Integrated fluorescence and transmission electron microscopy. J Struct Biol 164: 183-9.

Aikens, R.S., D.A. Agard, and J.W. Sedat, 1989. Solid-state imagers for microscopy. Methods Cell Biol 29: 291-313.

Armer, H.E., G. Mariggi, K.M. Png, C. Genoud, A.G. Monteith, A.J. Bushby, H. Gerhardt, and L.M. Collinson, 2009. Imaging transient blood vessel fusion events in zebrafish by correlative volume electron microscopy. PLoS One 4: e7716.

Barcena, M., and A.J. Koster, 2009. Electron tomography in life science. Semin Cell Dev Biol 20: 920-30.

Baumeister, W., and A.C. Steven, 2000. Macromolecular electron microscopy in the era of structural genomics. Trends Biochem Sci 25: 624-31.

Betzig, E., G.H. Patterson, R. Sougrat, O.W. Lindwasser, S. Olenych, J.S. Bonifacino, M.W. Davidson, J. Lippincott-Schwartz, and H.F. Hess, 2006. Imaging intracellular fluorescent proteins at nanometer resolution. Science 313: 1642-5.

Briegel, A., S. Chen, A.J. Koster, J.M. Plitzko, C.L. Schwartz, and G.J. Jensen, 2010. Correlated light and electron cryo-microscopy. Methods Enzymol 481: 317-41.

Chiu, W., M.L. Baker, W. Jiang, M. Dougherty, and M.F. Schmid, 2005. Electron cryomicroscopy of biological machines at subnanometer resolution. Structure 13: 363-72.

Cohen, B.E., A. Pralle, X. Yao, G. Swaminath, C.S. Gandhi, Y.N. Jan, B.K. Kobilka, E.Y. Isacoff, and L.Y. Jan, 2005. A fluorescent probe designed for studying protein conformational change. Proc Natl Acad Sci U S A 102: 965-70.

Frey, T.G., G.A. Perkins, and M.H. Ellisman, 2006. Electron tomography of membrane-bound cellular organelles. Annu Rev Biophys Biomol Struct 35: 199-224.

Grigorieff, N., and S.C. Harrison, 2011. Near-atomic resolution reconstructions of icosahedral viruses from electron cryo-microscopy. Curr Opin Struct Biol 21: 265-73.

Gruska, M., O. Medalia, W. Baumeister, and A. Leis, 2008. Electron tomography of vitreous sections from cultured mammalian cells. J Struct Biol 161: 384-92.

Hayles, M.F., D.A. Matthijs de Winter, C.T. Schneijdenberg, J.D. Meeldijk, U. Luecken, H. Persoon, J. de Water, F. de Jong, B.M. Humbel, and A.J. Verkleij, 2010. The making of frozen-hydrated, vitreous lamellas from cells for cryo-electron microscopy. J Struct Biol 172: 180-90.

Hell, S.W., 2003. Toward fluorescence nanoscopy. Nat Biotechnol 21: 1347-55.

Hell, S.W., and J. Wichmann, 1994. Breaking the diffraction resolution limit by stimulated emission: stimulated-emission-depletion fluorescence microscopy. Opt Lett 19: 780-2.

Hoffmann, A., F. Kulzer, R. Zondervan, J. Kohler, and M. Orrit, 2008. Single Biomolecules at Cryogenic Temperatures: From Structure to Dynamics in: R. Rigler and H. Vogel, Eds.), Single Molecules and Nanotechnology, Springer Berlin.

Koning, R.I., and A.J. Koster, 2009. Cryo-electron tomography in biology and medicine. Ann Anat 191: 427-45.

Koster, A.J., and J. Klumperman, 2003. Electron microscopy in cell biology: integrating structure and function. Nat Rev Mol Cell Biol Suppl: SS6-10.

Kukulski, W., M. Schorb, S. Welsch, A. Picco, M. Kaksonen, and J.A. Briggs, 2011. Correlated fluorescence and 3D electron microscopy with high sensitivity and spatial precision. J Cell Biol 192: 111-9.

Le Gros, M.A., G. McDermott, M. Uchida, C.G. Knoechel, and C.A. Larabell, 2009. High-aperture cryogenic light microscopy. J Microsc 235: 1-8.

Lepper, S., M. Merkel, A. Sartori, M. Cyrklaff, and F. Frischknecht, 2010. Rapid quantification of the effects of blotting for correlation of light and cryo-light microscopy images. J Microsc 238: 21-6.

Lucic, V., F. Forster, and W. Baumeister, 2005. Structural studies by electron tomography: from cells to molecules. Annu Rev Biochem 74: 833-65.

Lucic, V., A.H. Kossel, T. Yang, T. Bonhoeffer, W. Baumeister, and A. Sartori, 2007. Multiscale imaging of neurons grown in culture: from light microscopy to cryo-electron tomography. J Struct Biol 160: 146-56.

Marko, M., C. Hsieh, R. Schalek, J. Frank, and C. Mannella, 2007. Focused-ion-beam thinning of frozen-hydrated biological specimens for cryo-electron microscopy. Nat Methods 4: 215-7.

McIntosh, R., D. Nicastro, and D. Mastronarde, 2005. New views of cells in 3D: an introduction to electron tomography. Trends Cell Biol 15: 43-51.

Moerner, W.E., and M. Orrit, 1999. Illuminating single molecules in condensed matter. Science 283: 1670-6.

Nixon, S.J., R.I. Webb, M. Floetenmeyer, N. Schieber, H.P. Lo, and R.G. Parton, 2009. A single method for cryofixation and correlative light, electron microscopy and tomography of zebrafish embryos. Traffic 10: 131-6.

Orrit, M., 2002. Single molecules. Molecular entanglements. Science 298: 369-70.

Patterson, G., M. Davidson, S. Manley, and J. Lippincott-Schwartz, 2010. Superresolution imaging using single-molecule localization. Annu Rev Phys Chem 61: 345-67.

Peters, P.J., and J. Pierson, 2008. Immunogold labeling of thawed cryosections. Methods Cell Biol 88: 131-49.

Rigort, A., F.J. Bauerlein, A. Leis, M. Gruska, C. Hoffmann, T. Laugks, U. Bohm, M. Eibauer, H. Gnaegi, W. Baumeister, and J.M. Plitzko, 2010. Micromachining tools and correlative approaches for cellular cryo-electron tomography. J Struct Biol 172: 169-79.

Rust, M.J., M. Bates, and X. Zhuang, 2006. Sub-diffraction-limit imaging by stochastic optical reconstruction microscopy (STORM). Nat Methods 3: 793-5.

Sartori, A., R. Gatz, F. Beck, A. Rigort, W. Baumeister, and J.M. Plitzko, 2007. Correlative microscopy: bridging the gap between fluorescence light microscopy and cryo-electron tomography. J Struct Biol 160: 135-45.

Schwartz, C.L., V.I. Sarbash, F.I. Ataullakhanov, J.R. McIntosh, and D. Nicastro, 2007. Cryo-fluorescence microscopy facilitates correlations between light and cryo-electron microscopy and reduces the rate of photobleaching. J Microsc 227: 98-109.

Shu, X., V. Lev-Ram, T.J. Deerinck, Y. Qi, E.B. Ramko, M.W. Davidson, Y. Jin, M.H. Ellisman, and R.Y. Tsien, 2011. A genetically encoded tag for correlated light and electron microscopy of intact cells, tissues, and organisms. PLoS Biol 9: e1001041.

Sims, P., R. Albrecht, J.B. Pawley, V. Centonze, T. Deerinck, and J. Hardin, 2006. When Light Microscope Resolution Is Not Enough: Correlational Light Microscopy and Electron Microscopy, in: J. B. Pawley, (Ed.), Handbook of Biological Confocal Microscopy, Springer Science and Business Media, New York.

Sims, P.A., and J.D. Hardin, 2007. Fluorescence-integrated transmission electron microscopy images: integrating fluorescence microscopy with transmission electron microscopy. Methods Mol Biol 369: 291-308.

Slot, J.W., and H.J. Geuze, 2007. Cryosectioning and immunolabeling. Nat Protoc 2: 2480-91.

Thompson, R.E., D.R. Larson, and W.W. Webb, 2002. Precise nanometer localization analysis for individual fluorescent probes. Biophys J 82: 2775-83.

Truong, K., and M. Ikura, 2001. The use of FRET imaging microscopy to detect protein-protein interactions and protein conformational changes in vivo. Curr Opin Struct Biol 11: 573-8.

Vicidomini, G., M.C. Gagliani, M. Canfora, K. Cortese, F. Frosi, C. Santangelo, P.P. Di Fiore, P. Boccacci, A. Diaspro, and C. Tacchetti, 2008. High data output and automated 3D correlative light-electron microscopy method. Traffic 9: 1828-38.

Wang, Q., C.P. Mercogliano, and J. Lowe, 2011. A ferritin-based label for cellular electron cryotomography. Structure 19: 147-54.

Watanabe, S., A. Punge, G. Hollopeter, K.I. Willig, R.J. Hobson, M.W. Davis, S.W. Hell, and E.M. Jorgensen, 2010. Protein localization in electron micrographs using fluorescence nanoscopy. Nat Methods 8: 80-4.

Willig, K.I., R.R. Kellner, R. Medda, B. Hein, S. Jakobs, and S.W. Hell, 2006. Nanoscale resolution in GFP-based microscopy. Nat Methods 3: 721-3.

Zuber, B., M. Chami, C. Houssin, J. Dubochet, G. Griffiths, and M. Daffe, 2008. Direct visualization of the outer membrane of mycobacteria and corynebacteria in their native state. J Bacteriol 190: 5672-80.